

## Microstructure and Dynamics of Semicrystalline Poly(ethylene oxide)–Poly(vinyl acetate) Blends

Daniel Fragiadakis<sup>†</sup> and James Runt<sup>\*</sup>*Department of Materials Science and Engineering, The Pennsylvania State University, University Park, Pennsylvania 16802. <sup>†</sup>Current address: Naval Research Laboratory, Polymer Physics Section, Washington, DC 20375.**Received September 21, 2009; Revised Manuscript Received November 9, 2009*

**ABSTRACT:** The microstructure and dynamics of semicrystalline, melt-miscible poly(ethylene oxide)/poly(vinyl acetate) (PEO/PVAc) blends were investigated using small-angle X-ray scattering (SAXS) and broadband dielectric relaxation spectroscopy, respectively. PEO/PVAc blends with selected compositions were crystallized, and SAXS was used to determine the location of the noncrystallizable PVAc in the structure. Values of the microstructural parameters indicate that little, if any, PVAc is incorporated into interlamellar regions under these crystallization conditions, but PVAc diffuses to interfibrillar regions during the crystallization process. For crystalline blends, a dielectric relaxation appears in the same location as the neat PEO  $\alpha$ -process, indicating the presence of relatively mobile amorphous segments consisting almost entirely of PEO, in blends with compositions having as much as 50% PVAc. Considering the findings from the SAXS experiments, we attribute  $\alpha_{\text{PEO}}$  in the blends to the segmental process of the mobile portion of the interlamellar PEO segments. The shape of an observed higher temperature dielectric relaxation, particularly for blends with 30% and 50% PVAc content, suggests that it consists of multiple overlapping processes. The evidence suggests that these are a Maxwell–Wagner–Sillars (MWS) interfacial polarization process (similar to the one observed for neat PEO), a slow segmental process associated with amorphous interfibrillar regions, and possibly a second MWS relaxation.

## 1. Introduction

There has been considerable experimental and theoretical interest in the past decade in dynamic heterogeneity of miscible polymer mixtures, particularly miscible polymer blends exhibiting weak intermolecular interactions.<sup>1–6</sup> In situations where the intrinsic mobilities of the component polymers are significantly different (i.e., where the difference in dynamic glass transition temperatures ( $T_{\alpha}$ ) is  $> \sim 50$  °C), multiple  $\alpha$  processes are observed and indicative of local environments rich in the respective components. The Lodge–McLeish model interprets these observations in terms of the effect of chain connectivity on the local concentration experienced by a polymer segment.<sup>7</sup> Strong intermolecular associations (hydrogen bonding) between the components have been found to suppress concentration fluctuations and (at least) partially couple the segmental motions of the two components.<sup>8–10</sup>

The focus of the present work is on the dynamics of blends of weakly interacting polymers in which one of the components is capable of crystallization from the miscible melt state. This builds on our previous efforts on exploring the microstructure and crystallization kinetics of a series of “model” melt-miscible poly(ethylene oxide) [PEO] blends.<sup>11–13</sup> The dynamics of semicrystalline blends of melt-miscible polymers are rather complex, and there have been infrequent reports on this topic.<sup>14,15</sup> In addition to relatively mobile amorphous segments that relax at  $T_g$  (or  $T_{\alpha}$ ), it is well-known that segments in order–disorder interphases at crystal surfaces and some noncrystalline segments in interlamellar regions have significantly lower mobility than unconstrained amorphous segments and do not contribute to the heat capacity change at  $T_g$  or the relaxation strength of the dielectric  $\alpha$ -process

(these segments are collectively referred to as the rigid amorphous fraction).<sup>16,17</sup>

In the present paper, we report on our investigation of the dynamics of miscible PEO–poly(vinyl acetate) [PVAc] blends using broadband dielectric spectroscopy and focus principally on compositions from which a portion of the PEO crystallizes from the miscible melt at a fixed crystallization temperature. For background on the dynamics of amorphous PEO/PVAc mixtures, the reader is referred to refs 18 and 19 and references therein. The key to the interpretation of the relaxation behavior in semicrystalline materials is to first develop a detailed understanding of the microstructure in the blends. This was undertaken in the present case using primarily small-angle X-ray scattering experiments.

## 2. Experimental Section

**Materials.** Poly(vinyl acetate) was purchased from Alfa Aesar. It was fractionated using acetone and hexane as solvent and nonsolvent, respectively. The number-average molecular weight ( $M_n$ ) was determined using GPC to be 58 000 Da, with  $M_w/M_n = 1.6$ . Poly(ethylene oxide) ( $M_n = 25\,000$ ,  $M_w/M_n = 1.1$ ) was purchased from Polymer Source. The two components were dissolved in a common solvent, chloroform, and stirred for several hours. After casting onto Teflon-coated molds, the samples were left to dry overnight under ambient conditions and then dried under vacuum to ensure complete removal of the solvent. Blends containing 10, 30, 50, and 90 wt % PVAc were prepared. Samples of neat PEO and PVAc were also studied.

**Differential Scanning Calorimetry (DSC).** All DSC measurements were performed using a Seiko DSC 220 instrument. The samples were initially heated to 80 °C, well above the melting point, and held for 20 min to ensure complete melting. They were then quickly cooled to 44 °C and allowed to crystallize

<sup>\*</sup>Corresponding author. E-mail: [runt@matse.psu.edu](mailto:runt@matse.psu.edu).

isothermally. The crystallization process slows down with increasing PVAc content,<sup>12</sup> but a time of 2 h was found to be sufficient for crystallization to be complete for all materials. Subsequently, the samples were cooled to  $-100$  at  $10$  °C/min. Data were collected during the following heating scan at  $10$  °C/min up to  $100$  °C. Melting temperatures ( $T_m$ , peak), enthalpies, and glass transition temperatures ( $T_g$ ) from the midpoint of the heat capacity change were determined. Bulk crystallinities were determined based on a perfect heat of fusion of  $203$  J/g for PEO.<sup>20</sup>

**Small-Angle X-ray Scattering (SAXS).** SAXS measurements were carried out using a Molecular Metrology instrument equipped with a Cu K $\alpha$  radiation source ( $\lambda = 1.542$  Å) and a two-dimensional area proportional detector. The sample-to-detector distance was  $1.5$  m. Samples for SAXS were placed between two Teflon sheets and melted in a hydraulic press at  $80$  °C. They were then quickly transferred to a temperature-controlled hot plate where they were allowed to isothermally crystallize at  $44$  °C. The films thus obtained were cut into  $5$  mm  $\times$   $5$  mm squares, and several films were stacked to obtain a total sample thickness of ca.  $1$  mm. Scattering data were collected for  $90$  min.

Absolute scattered intensities (in units of  $\text{cm}^{-1}$ ) were determined by calibration with a precalibrated cross-linked polyethylene (S-2907) secondary standard. A silver behenate secondary standard was used to calibrate the scattering vector. Corrections for a constant scattering background due to thermal density fluctuations were made by evaluating the slope of an  $Iq^4$  vs  $q^4$  plot in the high- $q$  region and subtracting it from the overall  $I$  vs  $q$  data.<sup>21</sup>

The one-dimensional correlation function,  $G(r)$ , was calculated from the measured intensity vs  $q$  data:<sup>22</sup>

$$G(r) = \frac{1}{2\pi^2} \int_0^\infty q^2 I(q) \cos(qr) dq \quad (1)$$

where  $r$  is the correlation distance. Before applying eq 1,  $I$  vs  $q$  data were linearly extrapolated to  $q = 0$  and extrapolated to large  $q$  values according to Porod's law,  $I(q) \propto q^{-4}$ .<sup>21</sup>

**Dielectric Relaxation Spectroscopy (DRS).** Samples for DRS measurements were heated above the melting point and sandwiched between two polished brass electrodes, with the sample thickness kept constant at  $50$   $\mu\text{m}$  using silica spacers. The samples were then dried under vacuum ( $< 10^{-3}$  mbar) for  $24$  h prior to measurement.

A Novocontrol GmbH Concept 40 broadband dielectric spectrometer was used to measure the dielectric permittivity. The samples were quickly transferred to the cryostat, where thermal treatment and measurements were performed under a flow of dry  $\text{N}_2$ . The samples were initially held at  $80$  °C for  $20$  min and then cooled to  $44$  °C where they were crystallized isothermally. Crystallization was monitored by recording the change in conductivity and dielectric permittivity as a function of time. After crystallization was complete, the samples were cooled to  $-100$  °C, and measurements performed on subsequent heating up to  $60$  °C. Frequency sweeps were performed isothermally from  $10$  MHz to  $0.01$  Hz.

Dipolar relaxations were analyzed by fitting the dielectric loss  $\epsilon''$  or the so-called derivative spectra (in which the dielectric loss is determined from the dielectric constant to remove the contribution from conduction losses)<sup>23</sup> using the appropriate form of the Havriliak–Negami equation:<sup>24</sup>

$$\epsilon_{\text{HN}}^* = \frac{\Delta\epsilon}{[1 + (if/f_{\text{HN}})^a]^b}$$

for each relaxation process, where  $\Delta\epsilon$  is the relaxation strength,  $a$  and  $b$  are shape parameters, and  $f_{\text{HN}}$  is a characteristic frequency related to the frequency  $f_{\text{max}}$  of maximum

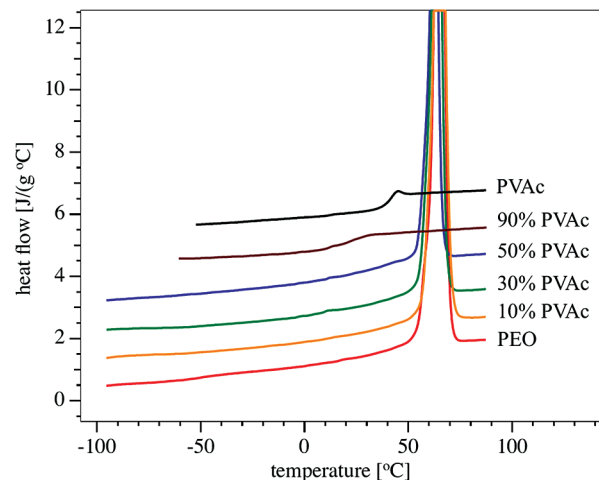


Figure 1. DSC heating scans for neat PEO and PEO/PVAc blends.

Table 1. Melting Temperature, Melting Enthalpy, and Degree of Crystallinity Normalized to the Weight Fraction of PEO

	$T_m$ (°C)	$\Delta H$ (J/g)	% crystallinity
PEO	65	154	76
10% PVAc	65	139	73
30% PVAc	64	123	77
50% PVAc	63	80	75

loss by

$$f_{\text{max}} = f_{\text{HN}} \left( \sin \frac{a\pi}{2+2b} \right)^{1/a} \left( \sin \frac{ab\pi}{2+2b} \right)^{-1/a}$$

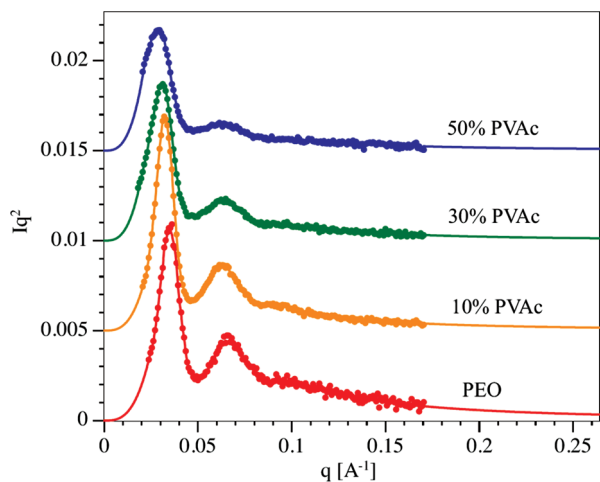
### 3. Results and Discussion

Figure 1 shows DSC heating scans, following isothermal crystallization at  $44$  °C. The neat PEO and blends with  $10$ ,  $30$ , and  $50\%$  PVAc are semicrystalline and display a single melting peak around  $65$  °C. Because of the high degree of crystallinity, a glass transition is not clearly discernible in any of the DSC curves of PEO or the semicrystalline blends. With increasing PVAc content, crystallization during the prior isothermal step (not shown) proceeds considerably more slowly due to the reduction in molecular mobility and dilution with PVAc. However, the degrees of crystallinity of the blends, normalized to the concentration of PEO in each blend (Table 1), are the same within experimental error of neat PEO. The melting temperature decreases only slightly, from  $65$  to  $63$  °C, suggesting that the equilibrium characteristics of PEO are not significantly altered by the presence of the diluent.

PVAc exhibits a single  $T_g$  around  $35$  °C. The blend containing  $90\%$  PVAc shows no evidence of crystallinity and exhibits only one visible  $T_g$ , at a lower temperature than that of PVAc. Note that a single glass transition, as is observed for the  $90\%$  PVAc blend, is often taken to indicate a completely miscible mixture, but the reverse is not always true; multiple  $T_g$ s (or  $T_{\text{os}}$ ) have been reported for miscible blends of PVAc with PEO oligomers at lower PVAc content<sup>25</sup> and, as noted earlier, for a significant number of miscible blends exhibiting weak intermolecular interactions.<sup>1–6</sup>

**3.1. Structure.** Figure 2 displays the experimental SAXS curves for PEO and the semicrystalline blends. We observe a well-defined scattering peak corresponding to the long period ( $L$ ) of the lamellar structure,  $L = 2\pi/q_{\text{max}}$ . A reflection is clearly visible at  $q = 2q_{\text{max}}$  and a faint additional one at  $q = 3q_{\text{max}}$ , indicating a well-ordered lamellar morphology.

The calculated one-dimensional correlation functions are displayed in Figure 3. From the analysis of the



**Figure 2.** Lorentz-corrected SAXS intensities. The lines are the extrapolated intensities used in the calculation of the correlation function, as described in the Experimental Section.

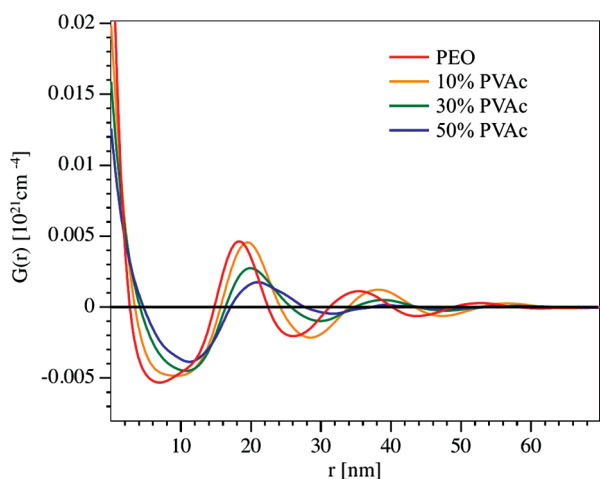


**Figure 3.** Calculated correlation functions for neat PEO and semicrystalline PEO/PVAc blends.

self-correlation triangle centered on  $q = 0$ , one can determine the main structural parameters of the lamellar stacks. The value of  $G(r)$  at  $r = 0$ , the invariant ( $Q_{\text{fit}}$ ), is given by<sup>26</sup>

$$Q_{\text{fit}} = i_e N_A^2 v_s w_c (1 - w_c) \Delta \eta^2 \quad (2)$$

where  $w_c$  is the linear crystallinity [ratio of the lamellar thickness  $l_c$  to the long period ( $L = l_c + l_a$ )],  $v_s$  is the volume fraction of lamellar stacks,  $\Delta \eta$  is the linear electron density difference between crystalline lamella and polymer segments in the interlamellar regions, and  $i_e = 7.94 \times 10^{-26} \text{ cm}^2$  is the Thomson differential cross section of a single electron. (In units of  $\text{cm}^{-4}$ . This differs from the expression used by Strobl et al.,<sup>22</sup> who use units of  $(\text{mol electron}/\text{cm}^3)^2$ , by the factor  $i_e N_A^2$ ).

The intersection point of the linear fit with  $G(r) = 0$  is (for  $w_c > 0.5$ )

$$r_0 = w_c (1 - w_c) L = \langle l_c \rangle (1 - w_c) = \langle l_a \rangle w_c \quad (3)$$

and the baseline is at

$$A = Q_{\text{fit}} \frac{1 - w_c}{w_c} \quad (4)$$

**Table 2. Structural Parameters Obtained from Analysis of the SAXS Correlation Function**

	PEO	10% PVAc	30% PVAc	50% PVAc
linear crystallinity ( $w_c$ )	0.82	0.79	0.78	0.78
bulk crystallinity (DSC)	0.76	0.66	0.54	0.38
crystal thickness, $l_c$ [nm]	14.9	15.4	15.6	16.4
amorph layer thickness, <sup>a</sup> $l_a$ [nm]	3.4	4.1	4.3	4.6
long period, <sup>b</sup> $L$ [nm]	17.9	19.6	20.2	21.5
long period, <sup>c</sup> $L$ [nm]	18.3	19.5	19.9	21

<sup>a</sup> Estimated experimental uncertainty is 0.5 nm. <sup>b</sup> From peak of Lorentz-corrected scattering intensity. <sup>c</sup> From first maximum of correlation function.

The parameters  $Q_{\text{fit}}$  and  $r_0$  are obtained directly from a linear fit to the self-correlation portion of  $G(r)$ . The value of one additional parameter is needed to completely determine the structure using eqs 2–4. Either the value of the baseline,  $A$ , or the long period  $L$  can be used. We avoid using the baseline since this approach is only reliable if we assume *a priori* that  $w_c < 0.3$  or  $w_c > 0.7$ .<sup>22</sup> Also, finite lamellar stacks (due to the presence of interfibrillar material) may make determination of  $A$  from the minimum of the correlation function unreliable (i.e., the minimum of the correlation function may be different than  $A$ ). We therefore use the long period. Strictly, the number-average value of  $L$  is required. The first correlation maximum yields the most probable value, while the Lorentz peak position gives the weight-average value.<sup>27,28</sup> Assuming a minimum distribution of long periods, we use the first maximum of the correlation function to determine  $L$ . The linear crystallinity and the amorphous and crystalline layer thicknesses are obtained from eq 3. The structural parameters obtained in this way are displayed in Table 2, along with the long periods from the Lorentz-corrected scattering curves (weight-average) and the first maximum of the correlation function (most probable value).

The linear crystallinity for neat PEO is equal to, within experimental error, the bulk crystallinity. This indicates a structure consisting of space-filling lamellar stacks. With increasing PVAc content, the linear crystallinity remains relatively constant while the bulk crystallinity, determined from DSC data, decreases significantly, indicating the presence of polymer outside the lamellar stacks, i.e., interfibrillar or interspherulitic incorporation of PVAc. Optical microscopy shows space-filling spherulites, ruling out significant interspherulitic PVAc.

The long periods determined from the first maximum of the correlation function and from the first peak in the Lorentz-corrected scattering intensity are the same within experimental error. The long period increases slightly with increasing PVAc content; however, the increase is very small compared to that expected for all-interlamellar incorporation of the PVAc (Figure 4). Analysis of the calculated correlation functions demonstrates that this increase arises from an increase in crystal thickness and perhaps a small increase in the thickness of the interlamellar amorphous layer (Figure 5). It should be noted that reported  $l_a$ 's and other length parameters have estimated experimental uncertainties of 0.5 nm.

For an interaction parameter  $\chi \sim 0$ , we expect the crystal thickness, and the equilibrium melting temperature, to be independent of blend composition. The increase in crystal thickness with increasing PVAc content suggests a reduction in the degree of supercooling, i.e., a depression of the equilibrium melting temperature, as the fraction of PVAc increases. This is consistent with a small negative interaction parameter between PEO and PVAc proposed by Chen et al.<sup>29,30</sup>

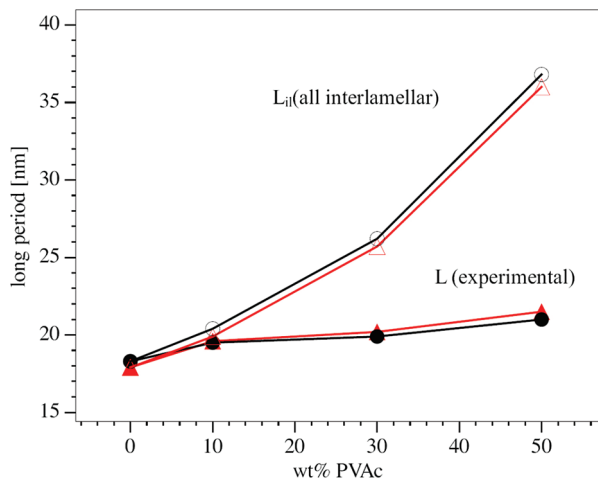


**Figure 4.** Experimental long periods calculated from the first maximum of the correlation function (circles) and the peak of the Lorentz-corrected scattering intensity (triangles), along with the corresponding calculated values of  $L$  for all-interlamellar location of PVAc.

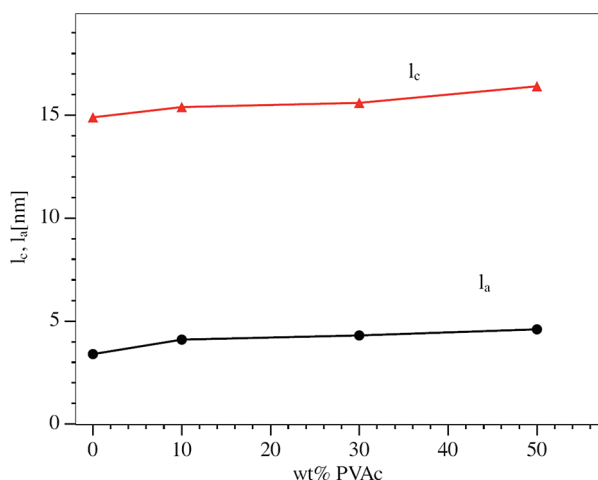


**Figure 5.** Crystal and amorphous layer thicknesses determined from the SAXS correlation function.

The very small apparent change in the thickness of the amorphous layer (Table 2) does not conclusively indicate whether there is some (small) interlamellar incorporation of PVAc. We attempt to determine this using the values of the invariant. We can calculate the theoretical values of the invariant for two limiting cases: In the case where all PVAc is incorporated into lamellar stacks, the linear crystallinity is equal to the bulk crystallinity, and the invariant is given by

$$Q_{il} = i_c N_A^2 \phi_c (1 - \phi_c) \Delta \eta^2 \quad (5)$$

In the case where all the PVAc is excluded into interfibrillar regions, the invariant is given by

$$Q_{if} = i_c N_A^2 (1 - \phi_d) \frac{\phi_c \phi_a}{\phi_c + \phi_a} \Delta \eta^2 \quad (6)$$

where  $\phi_a$ ,  $\phi_c$ , and  $\phi_d$  are the volume fractions of amorphous PEO, crystalline PEO, and PVAc, respectively. In Figure 6 we plot the experimental values of the invariant as well as the calculated invariants for the above extreme cases. The differences between the three are very small—much smaller than the experimental error. The main source of uncertainty

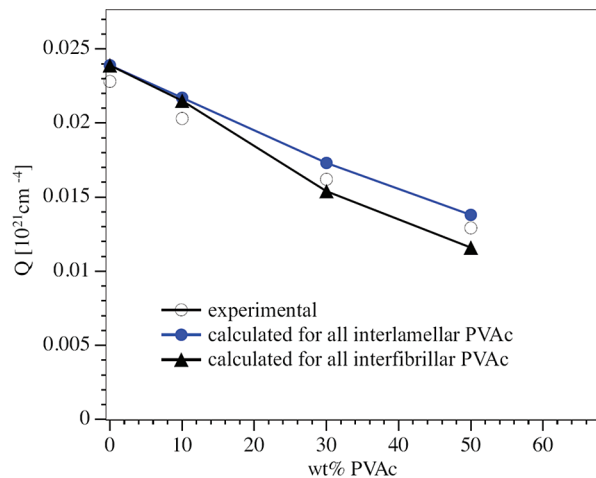


**Figure 6.** Experimental invariant  $Q_{fit}$  determined from the correlation function and calculated values of  $Q$  for all-interlamellar and all-interfibrillar location of PVAc.

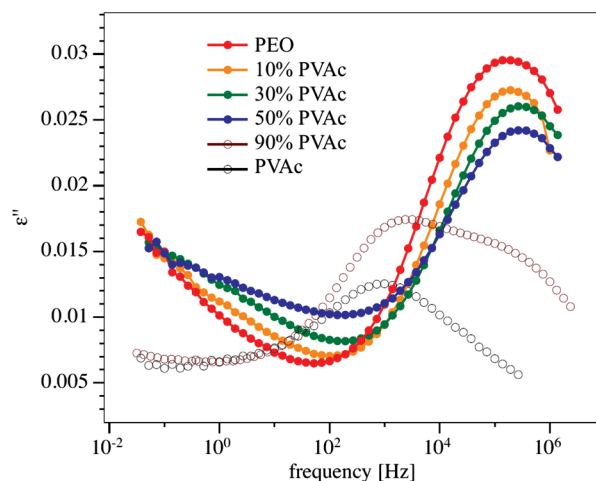


**Figure 7.** Representative dielectric loss vs frequency in the glassy state ( $-70^\circ\text{C}$ ).

is that the electron density of PVAc falls between those of amorphous and crystalline PEO.<sup>13</sup> Since all three densities are very similar, even small uncertainties in the values of the mass densities yield large errors in the calculated invariant. Therefore, the analysis of the invariants cannot provide further information on the location of the PVAc phase. However, the behavior of the structural parameters ( $L$ ,  $l_a$ ,  $l_c$ ) and the linear crystallinity indicates that little, if any, PVAc is incorporated into interlamellar regions.

**3.2. Dynamics. Local Dynamics.** Figure 7 shows dielectric loss spectra of the materials under investigation at  $-70^\circ\text{C}$ . PEO displays a single, broad  $\beta_{PEO}$  process around  $10^5$  Hz, associated with local chain twisting of PEO segments, predominantly in the amorphous phase.<sup>31</sup> PVAc shows a single  $\beta_{PVAc}$  process, involving motions of the  $-\text{OCOCH}_3$  side groups. Both the amorphous and semicrystalline blends exhibit these two relaxations, their relaxation strengths varying in rough proportion to the fraction of amorphous PEO and PVAc in each blend. No significant shifting of the local processes occurs and no new local processes appear.

An additional local process, labeled  $\beta'$  in Figure 8, has been observed in nominally well-dried semicrystalline PEO,<sup>31</sup> PEO/poly(methyl methacrylate) [PMMA] blends,<sup>32</sup> and amorphous PEO/PVAc blends<sup>33</sup> at frequencies lower than  $\beta_{PEO}$ . This process has been related to constrained

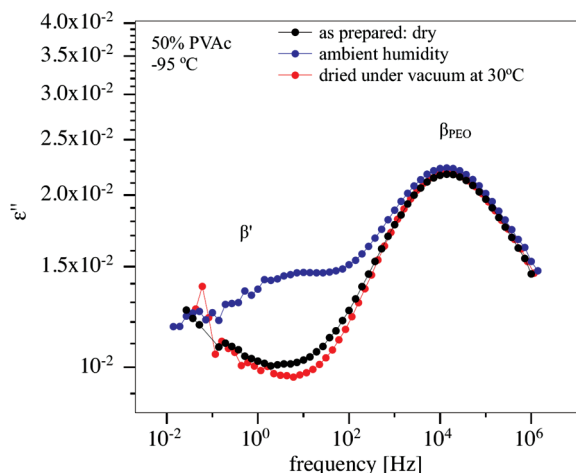


**Figure 8.** Effect of water on local dynamics. Dielectric loss spectra of 50% PVAc semicrystalline blend immediately after drying and crystallization, after exposure to ambient humidity, and after redrying under vacuum.

dynamics of PEO chains in the transition region between crystalline lamellae and interlamellar amorphous PEO as well as to the initial stages of crystallization in the otherwise apparently amorphous, PEO/PMMA and PEO/PVAc blends. A process in the same frequency and temperature range was observed in PEO-layered silicate nanocomposites,<sup>34,35</sup> where it was assigned to the segmental relaxation of nanoconfined PEO. Such a process is not observed for either neat PEO or the PEO/PVAc samples studied here. Therefore, we reexamine the influence of water content on local relaxation in PEO and the blends.

The measurements of Figure 7 were carried out immediately after drying the samples in vacuum. Both the isothermal crystallization and dielectric measurements were performed under a dry N<sub>2</sub> flow. Figure 8 shows the original dielectric loss spectra for the 50/50 PEO/PVAc blend immediately after drying and isothermal crystallization, as well as subsequent additional measurements of the same sample after exposure to ambient humidity, and after redrying at room temperature ( $< 10^{-3}$  mbar). An additional local process ( $\beta'$ ) appears when water is adsorbed, as a pronounced shoulder on the low-frequency side of the  $\beta_{\text{PEO}}$  process, and disappears again upon drying. This process has an Arrhenius temperature dependence with an activation energy of 52 kJ/mol, similar to the additional process previously observed in neat PEO, PEO/PMMA, and PEO/PVAc blends. Clearly, however, the  $\beta'$  process in the samples under investigation here is associated with the presence of water. It may be due to either reorientational motions of the water molecules themselves or local motions of the polymer chains (of the type that give rise to the  $\beta$  process), involving also the motion of one or more attached water molecules (thus slowing down the relaxation and increasing its activation energy). A relaxation in this temperature and frequency range with very similar characteristics, i.e., an Arrhenius temperature dependence below  $T_g$  and an activation energy of ca. 50 kJ/mol, has been observed in a wide variety of systems containing water. These range from mixtures of water with other small molecules and polymers, to polymers and biological systems containing small quantities of water, to water confined in nanoporous environments or adsorbed on surfaces.<sup>36–38</sup> This suggests the assignment of the  $\beta'$  process to reorientational motions of the water molecules themselves.

**Segmental Dynamics: Amorphous Blend.** The amorphous blend, containing 90% PVAc, shows a single segmental

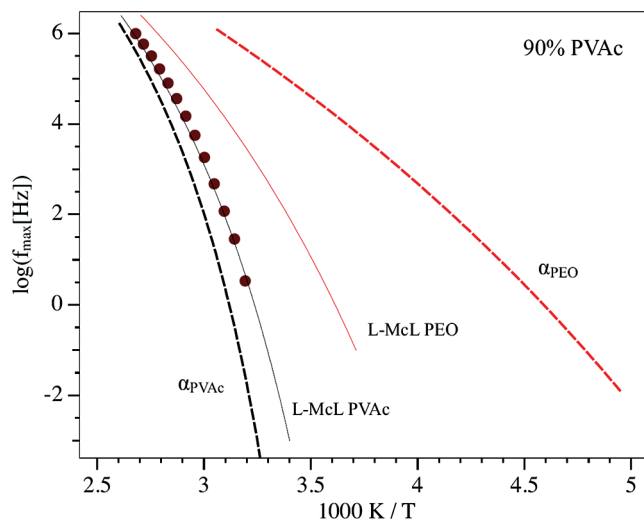


**Figure 9.** Arrhenius plot of the segmental relaxation of the 90% PVAc amorphous blend. Dashed lines correspond to the segmental processes of neat PEO and PVAc; dotted lines correspond to the prediction of the Lodge–McLeish model for the two segmental processes of the blend. Points are experimental data for the single segmental process of the blend.

process, faster and broader than the segmental process of neat PVAc. PEO and PVAc have a large difference in  $T_g$ s, and the interaction between the two components is weak. In dynamically asymmetric, weakly interacting miscible blends, the dynamics of the two components are often observed to be decoupled, resulting in two segmental relaxations even in a blend that is homogeneous at the molecular scale. The Lodge–McLeish model interprets this observation in terms of the effect of chain connectivity on the local concentration seen by a polymer segment.<sup>7</sup> In a blend of two polymers A and B, with volume fractions  $\phi_A$  and  $\phi_B$ , this local effective concentration of a segment of polymer A is

$$\phi_{\text{eff},A} = \phi_{s,A} + (1 - \phi_{s,A})\phi_A$$

(and similarly for polymer B).  $\phi_s$  is the so-called self-concentration, a constant for a given polymer, and is given by

$$\phi_s = \frac{C_\infty M_0}{k\rho N_{\text{av}}V}$$

where  $M_0$  is the repeat unit molar mass,  $k$  the number of backbone bonds per repeat unit, and  $\rho$  the density. The calculated value of  $\phi_s$  is 0.26 for PEO and 0.23 for PVAc, using the following input parameters:  $M_0 = 86.1$  g/mol,  $k = 2$ ,  $C$  (characteristic ratio) = 8.79,<sup>19</sup> the Kuhn length = 1.36 nm,<sup>19</sup> and  $\rho = 1.19$  g/cm<sup>3</sup>.<sup>39</sup> An effective  $T_g$  (or  $T_\alpha$ ) can then be calculated for each component, assuming it follows the Fox equation as a first approximation:

$$\frac{1}{T_{g,A}^{\text{eff}}} = \frac{\phi_{\text{eff}}}{T_{g,A}} + \frac{1 - \phi_{\text{eff}}}{T_{g,B}} \quad (7)$$

By substituting the frequency positions of the segmental processes of the neat PEO and PVAc into eq 7, one can estimate the expected location of the two segmental processes ( $\alpha_{\text{PEO}}$  and  $\alpha_{\text{PVAc}}$ ) predicted by the model for the amorphous 90% PVAc blend. The observed segmental relaxation,  $\alpha$ , is in good agreement with the Lodge–McLeish prediction for the slow component (Figure 9). This is in

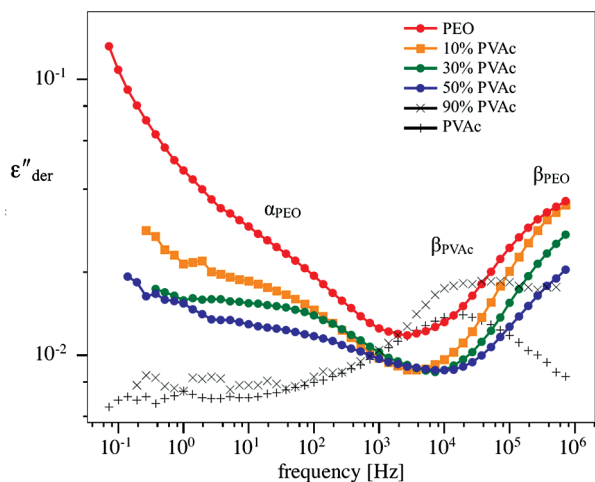


**Figure 10.** Derivative spectra of PEO, PVAc, and their blends at  $-40\text{ }^{\circ}\text{C}$ .

agreement with recent dielectric studies of PEO/PVAc blends<sup>33,40</sup> where a single segmental relaxation was observed reflecting primarily the mobility of the PVAc component. There is no indication in the spectra of a faster  $\alpha_{\text{PEO}}$  segmental process, even as a slight change of slope or shoulder. Although the Lodge–McLeish model does not predict the relative relaxation strength of the two expected processes, we would expect  $\alpha_{\text{PEO}}$  for a blend containing only 10% PEO to be very weak, and its existence cannot therefore be ruled out.

*Segmental Dynamics: PEO and Semicrystalline Blends.* Above the glass transition temperature, the dielectric loss of PEO and the semicrystalline blends is dominated by dc conductivity. The derivative formalism<sup>23</sup> is therefore employed which allows the underlying relaxation processes to be better resolved. Derivative spectra at  $-40\text{ }^{\circ}\text{C}$  are displayed in Figure 10 and an isochronal representation at 20 Hz in Figure 11. The segmental process of PEO is visible as a shoulder around 50 Hz. In the blends, a process appears in the same location, within experimental error, as the segmental process of neat PEO. Relaxation strengths and shape parameters cannot be reliably extracted from the data due to significant overlap with the  $\beta_{\text{PVAc}}$  and Maxwell–Wagner–Sillars (MWS) processes; however, the relaxation strength of the  $\alpha_{\text{PEO}}$  process appears to decrease systematically with increasing PVAc content.

The fact that the PEO segmental process does not shift with increasing PVAc content (Figure 12) indicates the presence of relatively mobile amorphous regions consisting almost entirely of PEO, in blends with composition even as high as 50%. Even small amounts of mixing with PVAc would lead to a detectable shift in the frequency of the  $\alpha$ -process, due to the large difference ( $70\text{--}80\text{ }^{\circ}\text{C}$ ) in  $T_g$ s of the two polymers. Considering the findings from the SAXS data, which indicate minimal or no incorporation of PVAc into interlamellar regions, we attribute the  $\alpha_{\text{PEO}}$  process in the blends to the segmental process of the mobile portion of PEO segments in interlamellar regions.

Since the fast  $\alpha_{\text{PEO}}$  relaxation reflects the interlamellar component in the blends, we expect a second, slower  $\alpha$ -process corresponding to the segmental dynamics of the interfibrillar regions, which will consist primarily of PVAc and, for the 30% and 50% PVAc blends, constitute a significant fraction of the material. However, we are not able to resolve such a relaxation (see Figure 11). Instead, a strong, very broad relaxation process appears for both neat

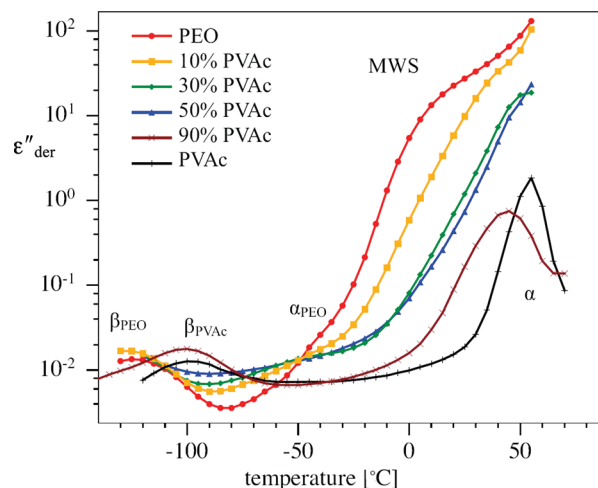


**Figure 11.**  $\epsilon''_{\text{der}}$  vs temperature at 20 Hz for PEO, PVAc, and the PEO/PVAc blends.

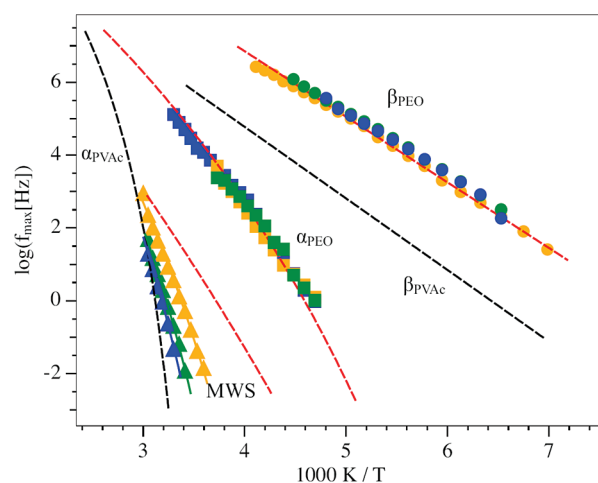


**Figure 12.** Arrhenius plot for the semicrystalline blends. Dashed lines correspond to the relaxation frequencies for neat PEO and PVAc.

PEO and the semicrystalline blends. This process is not present in PVAc or the amorphous 90% PVAc blend. For neat PEO the relaxation frequency of this process is proportional to that of the segmental relaxation of the amorphous interlamellar PEO. The relaxation strength of this process is of the order of 50—too large to be attributed to dipolar motions. We therefore initially attribute this process to a Maxwell–Wagner–Sillars polarization.<sup>41</sup> This is expected to arise from charge buildup at the interfaces between the crystalline lamellae and amorphous interlamellar regions, the latter having much higher conductivity and dielectric constant than the former.

With increasing PVAc, the MWS relaxation shifts to lower frequencies, broadens, and decreases in strength. The temperature dependence of the relaxation time changes and becomes gradually steeper, diverging from that of the  $\alpha$  process of the interlamellar layer of PEO (Figure 12). The shape of the MWS peak in the isochronal plots (Figure 11), particularly for the 30% and 50% blends, suggests that the process has more than one component. Taking into account the structural data, this strongly suggests that the process we have labeled “MWS” consists of multiple overlapping peaks. Presumably, these are (a) a MWS peak similar to the one of neat PEO, (b) the slow segmental process of the interfibrillar region, and perhaps (c) a second MWS peak, if the

interfibrillar phase has conductivity sufficiently different from those of both crystalline PEO and from amorphous PEO. Process (a) is the fastest component; the shift of the overall "MWS" peak to lower frequencies reflects the increased influence of (b), and potentially (c), with increasing PVAc content.

#### 4. Summary

In the present study, we first determine the details of the microstructure of selected melt-miscible PEO/PVAc blends with SAXS, utilizing the 1D correction function and invariant. With increasing PVAc content, the linear crystallinity remains constant while the bulk crystallinity decreases significantly, indicating the presence of PVAc outside of lamellar stacks. As the crystalline blends exhibit a volume filling spherulitic morphology and there is little change in the thickness of the amorphous interlamellar layers, little, if any, PVAc is incorporated into interlamellar regions but diffuses to interfibrillar zones during crystallization.

For crystalline PEO/PVAc blends, a process appears in the same location as the segmental process of neat crystalline PEO. This relaxation does not shift with increasing PVAc content, indicating the presence of relatively mobile amorphous segments consisting almost entirely of PEO. Considering the findings from the SAXS data, the  $\alpha_{\text{PEO}}$  process in the blends is attributed to the segmental process of a portion of the PEO interlamellar segments. The shape of the higher temperature relaxation, particularly for the 30% and 50% blends, suggests that it consists of more than one process, and we hypothesize regarding its origin.

**Acknowledgment.** The authors gratefully acknowledge the support of the National Science Foundation, Polymers Program, under Grants DMR-0605627 and DMR-0907139.

#### References and Notes

- Mpoukouvalas, K.; Floudas, G. *Macromolecules* **2008**, *41*, 1552.
- Kumar, S. K.; Shenogin, S.; Colby, R. H. *Macromolecules* **2007**, *40*, 5759.
- Hirose, Y.; Adachi, K. *Macromolecules* **2006**, *39*, 1779.
- Roland, C. M.; McGrath, K. J.; Casalini, R. *Macromolecules* **2006**, *39*, 3581.
- Farago, B.; Chen, C. X.; Maranas, J. K.; Kamath, S.; Colby, R. H.; Pasquale, A. J.; Long, T. E. *Phys. Rev. E* **2005**, *7203*, 1809.
- Sy, J. W.; Mijovic, J. *Macromolecules* **2000**, *33*, 933.
- Lodge, T. P.; Mcleish, T. C. B. *Macromolecules* **2000**, *33*, 5278.
- Masser, K. A.; Runt, J. *Macromol. Symp.* **2009**, *279*, 221.
- Runt, J.; Zhang, S. H. In *Structure and Dynamics in Macromolecular Systems with Specific Interactions*; Adachi, K., Sato, T., Eds.; Osaka University Press: Osaka, 2005; p 181.
- Zhang, S. H.; Runt, J.; Casalini, R.; Roland, C. M. *Macromolecules* **2003**, *36*, 9917.
- Cho, J. D.; Xu, R.; Yeh, F.; Hsiao, B. S.; Runt, J. *Macromol. Symp.* **2003**, *198*, 29.
- Wu, L.; Lisowski, M.; Talibuddin, S.; Runt, J. *Macromolecules* **1999**, *32*, 1576.
- Talibuddin, S.; Wu, L.; Runt, J.; Lin, J. S. *Macromolecules* **1996**, *29*, 7527.
- Linares, A.; Nogales, A.; Rueda, D. R.; Ezquerro, T. A. *J. Polym. Sci., Polym. Phys.* **2007**, *45*, 1653.
- Ren, J.; Adachi, K. *Macromolecules* **2003**, *36*, 5180.
- Wunderlich, B. *Prog. Polym. Sci.* **2003**, *28*, 383.
- Lu, S. X.; Cebe, P. *Polymer* **1996**, *37*, 4857.
- Zhao, J.; Zhang, L.; Ediger, M. D. *Macromolecules* **2008**, *41*, 8030.
- Tyagi, M.; Arbe, A.; Alegria, A.; Colmenero, J.; Frick, B. *Macromolecules* **2007**, *40*, 4568.
- Wunderlich, B. *Macromolecular Physics*; Academic Press: New York, 1980; Vol. 3.
- Ruland, W. *J. Appl. Crystallogr.* **1971**, *4*, 70.
- Strobl, G. R.; Schneider, M.; Voigt-Martin, I. *J. Polym. Sci., Polym. Phys. Ed.* **1980**, *19*, 1361.
- Wübbenhorst, M.; van Turnhout, J. *J. Non-Cryst. Solids* **2002**, *305*, 40.
- Havriliak, S.; Negami, S. *J. Polym. Sci., Polym. Symp.* **1966**, *14*, 99.
- Gaikwad, A. N.; Wood, E. R.; Ngai, T.; Lodge, T. P. *Macromolecules* **2008**, *41*, 2502.
- Elsner, G.; Koch, M. H. J.; Bordas, J.; Zachmann, H. G. *Makromol. Chem.* **1981**, *182*, 1263.
- Strobl, G. R.; Schneider, M. *J. Polym. Sci., Polym. Phys. Ed.* **1980**, *18*, 1343.
- Vonk, C. G. *J. Appl. Crystallogr.* **1978**, *11*, 541.
- Chen, X.; An, L. J.; Li, L. X.; Yin, J. H.; Sun, Z. Y. *Macromolecules* **1999**, *32*, 5905.
- Chen, X.; Yin, J. H.; Alfonso, G. C.; Pedemonte, E.; Turturro, A.; Gattiglia, E. *Polymer* **1998**, *39*, 4929.
- Jin, X.; Zhang, S. H.; Runt, J. *Polymer* **2002**, *43*, 6247.
- Jin, X.; Zhang, S. H.; Runt, J. *Macromolecules* **2004**, *37*, 8110.
- Tyagi, M.; Arbe, A.; Colmenero, J.; Frick, B.; Stewart, J. R. *Macromolecules* **2006**, *39*, 3007.
- Chrissopoulou, K.; Afratis, A.; Anastasiadis, S. H.; Elmahd, M. M.; Floudas, G.; Frick, B. *Eur. Phys. J. E* **2007**, *141*, 267.
- Elmahdy, M. M.; Chrissopoulou, K.; Afratis, A.; Floudas, G.; Anastasiadis, S. H. *Macromolecules* **2006**, *39*, 5170.
- Capaccioli, S.; Ngai, K. L.; Shinyashiki, N. *J. Phys. Chem. B* **2007**, *111*, 8197.
- Cervený, S.; Schwartz, G. A.; Bergman, R.; Swenson, J. *Phys. Rev. Lett.* **2004**, *93*, 245702.
- Cervený, S.; Alegria, A.; Colmenero, J. *Phys. Rev. E* **2008**, *77*, 031803.
- Brandrup, J.; Immergut, E. H.; Grulke, E. A.; Abe, A.; Bloch, D. R. *Polymer Handbook*; Wiley-Interscience: New York, 1999.
- Urakawa, O.; Ujii, T.; Adachi, K. *J. Non-Cryst. Solids* **2006**, *352*, 5042.
- (a) Maxwell, J. C. *Electricity and Magnetism*; Clarendon Press: Oxford, UK, 1892; Vol. 1. (b) Wagner, K. W. *Arch. Elektrotech.* **1914**, *2*, 378. (c) Sillars, R. W. *J. Inst. Electron. Eng.* **1937**, *80*, 378.